The role of substrate topography on the cellular uptake of nanoparticles

Changjin Huang,[1]* Tugba Ozdemir,[2]* Li-Chong Xu,[3] Peter J. Butler,[2] Christopher A. Siedlecki,[2,3] Justin L. Brown,[2] Sulin Zhang[1,2]

[1]Department of Engineering Science and Mechanics, The Pennsylvania State University, University Park, Pennsylvania 16802
[2]Department of Bioengineering, The Pennsylvania State University, University Park, Pennsylvania 16802
[3]Department of Surgery, The Pennsylvania State University, College of Medicine, Hershey, Pennsylvania 17033

Abstract: Improving targeting efficacy has been a central focus of the studies on nanoparticle (NP)-based drug delivery nanocarriers over the past decades. As cells actively sense and respond to the local physical environments, not only the NP design (e.g., size, shape, ligand density, etc.) but also the cell mechanics (e.g., stiffness, spreading, expressed receptors, etc.) affect the cellular uptake efficiency. While much work has been done to elucidate the roles of NP design for cells seeded on a flat tissue culture surface, how the local physical environments of cells mediate uptake of NPs remains unexplored, despite the widely known effect of local physical environments on cellular responses *in vitro* and disease states *in vivo*. Here, we report the active responses of human osteosarcoma cells to fibrous substrate topographies and the subsequent changes in the cellular uptake of NPs. Our experiments demonstrate that surface topography modulates cellular uptake efficacy by mediating cell spreading and membrane mechanics. The findings provide a concrete example of the regulative role of the physical environments of cells on cellular uptake of NPs, therefore advancing the rational design of NPs for enhanced drug delivery in targeted cancer therapy. © 2015 Wiley Periodicals, Inc. J Biomed Mater Res Part B: Appl Biomater 00B: 000–000, 2015.

Key Words: topographies, nanoparticles, endocytosis, fibers, scaffolds

How to cite this article: Huang C, Ozdemir T, Xu L, Butler PJ, Siedlecki C, Brown JL, Zhang S. 2015. The role of substrate topography on the cellular uptake of nanoparticles. J Biomed Mater Res Part B 2015:00B:000–000.

INTRODUCTION

Nanoparticle (NP)-based diagnostic and therapeutic agents are being considered as a revolutionary breakthrough in cancer treatments for their high targeting specificity and efficiency. Well-controlled delivery of NP-based bioagents into cancer cells can be achieved by tailoring NP size,[1–6] shape,[7–9] surface ligand density,[10–13] and so forth. Recent studies[14–18] evidenced that not only NP design, but also the local microenvironments are capable of modulating the cellular uptake of NPs. It has been well documented that a large variety of cell types actively sense surface topography and respond by altering their adhesion,[19–21] migration,[22–24] proliferation,[25–27] and differentiation.[28–30] Despite the intimate relations between cell function and surface topography, it remains unclear whether and how surface topography affects cellular uptake of NPs.

Since surface topography modulated cell responses were first brought into attention nearly half a century ago,[31] a large variety of topological features have emerged and been used as platforms to elicit desired cellular functions *in vitro*, including fibers, grooves, pillars, pits, and precisely controlled surface curvature and roughness.[26,28,32] Among all these topological features, the nanofibrous scaffolds may be the most physiologically relevant, considering the fibrous nature of extracellular matrices (ECMs) *in vivo*. The structures of ECMs vary in different tissues and undergo remodeling at different stages of development even within the same tissue, especially in cancer.[33] *In vitro* studies have demonstrated the capability of fibrous scaffolds in modulating cell functions. For example, it has been shown that aligned nanofibers induce unidirectional cell alignment similar to that found in native tissues (e.g., muscle, tendon, nerve and blood vessel).[34,35] Despite the fibrous nature of ECMs *in vivo*, *in vitro* experiments on evaluating the cellular uptake of NPs thus far have exclusively involved seeding cells on essentially flat surfaces (e.g., tissue culture-treated plates and petri dishes). As a result, the role of fibrous surface topography on the cellular uptake of NPs, despite its high biological relevance, remains unknown.

Herein, we fabricate poly(methyl methacrylate) (PMMA) fibrous substrates via electrospinning. The responses of human osteosarcoma SaOS-2 cells to substrate topography, characterized by fiber density, are characterized using fluorescence microscopy, atomic force microscopy (AFM), and a time-correlated single-photon counting (TCSPC) technique. Using fluorescent polystyrene NPs with a diameter of 100 nm, we show that substrate topography regulates cellular uptake of NPs by altering the extent of cell spreading and membrane mechanics. Using pharmacological inhibitors, we demonstrate that the relative significance of myosin II and stress fibers to the cellular uptake of NPs also varies on different substrate topographies. Our results shed light on the regulatory mechanisms involved in surface topography-mediated endocytosis of NPs, and therefore open a new dimension for the rational design of NP-based therapeutics with enhanced targeting efficiency.

MATERIALS AND METHODS

Substrate preparation
Completely smooth substrates were prepared by spin-coating 2% PMMA (MW 120,000; Sigma-Aldrich, St Louis, MO) dissolved in nitromethane (Sigma-Aldrich) on 22 mm × 22 mm glass slides at 2500 rpm for 15 s. Electrospinning with a stationary copper target was performed in order to generate PMMA fibrous substrates. Briefly, PMMA was dissolved in a 3:1 dimethylformamide (DMF):tetrahydrofuran (THF) solution at 25% w/v and was transferred to a 5-mL glass syringe with a 25G needle (Beckton Dickinson, Franklin Lanes, NJ). The syringe was placed on a syringe pump with the speed of pumping set to 5 mL/h. A 10 kV voltage was applied between the syringe tip and copper target and exposure time was adjusted between sparse and dense fiber deposition cases. Fibers were collected on glass coverslips placed 18 cm from the needle tip, which were precoated with 2% w/v Poly(2-hydroxyethyl methacrylate) (PHEMA; Sigma Aldrich) in 70% (v/v) ethanol through spin coating at 5000 rpm for 10 s. PHEMA prevents cell adhesion to nonfibrous regions. The desired densities of fibrous mesh were generated after 60 s and 10 s of electrospinning for dense and sparse fiber substrates, respectively. The fiber-deposited slides were then annealed by heating twice on a 120 °C hot plate for 1 min each. All substrates were UV-treated for minimum 30 min for sterilization prior to *in vitro* experiments. Following UV sterilization, both smooth and fibrous substrates were washed extensively with growth media for 15 min to eliminate cellular toxicity from possible solvent residues.

Substrate characterization
The surface topographies of both smooth and fibrous substrates were characterized using a scanning electron microscope (FEI Quanta 200, Philips, Netherlands). The average diameter (average of at least 100 measurements) of fibers was quantified through analysis of scanning electron microscopy (SEM) images using the National Institute of Health's ImageJ software package. The stiffness of the smooth PMMA layer and PMMA fibers was measured using

an AFM (NanoscopeIIIa, Digital Instruments, Santa Barbara, CA). The details of AFM tip preparation and data processing are published elsewhere.[15,36]

Cell culture
The human osteosarcoma cell line SaOS-2 was purchased from American Type Culture Collection (ATCC, Manassas, VA HTB-85). Cells were grown on 15 cm tissue culture grade polystyrene (TCPS) culture dishes (Sigma-Aldrich) in McCoy's 5A essential medium (ATCC, Manassas, VA), supplemented with 15% fetal bovine serum (FBS; Atlanta Biologicals, Lawrenceville, GA) and 1% penicillin–streptomycin (Pen-Strep; Invitrogen, Carlsbad, CA) at 37 °C in a 5% CO_2 atmosphere with 95% humidity. When they reached 80% confluence, cells were either detached from the surface using 0.05% trypsin–EDTA (Invitrogen, Carlbad, CA) and passed for tissue culture expansion or used for further experiments.

Fluorescence microscopy
Immunostaining was performed by staining F-actin, vinculin and nucleus following a previously published method.[37] Briefly, cells were fixed for 15 min in 3.7% paraformaldehyde followed by incubation with a permeabilization buffer, 3% bovine serum albumin and 0.1% Triton X-100 in phosphate-buffered saline (PBS), for 45 min. The cells were incubated with 1:1000 dilution of vinculin primary antibody (Sigma Aldrich) at room temperature for 1 h and with 1:500 dilution of Dyelight 488 secondary antibody (Rockland Immunochemicals, Gilbertsville, PA) for 45 min with extensive washing in between. Next, actin stress fibers were fluorescently labeled by incubating cells in a 1:1000 dilution of CF 568 conjugated phalloidin (Biotium, Hayward, CA) for 30 min. Nuclei were stained by incubating cells with a 1:5000 dilution of 4′-6-diamidino-2-phenylindole (DAPI; Pierce, Rockford, IL) for 5 min. The stained slides were mounted using ProLong Gold antifade reagent (Invitrogen, Eugene, OR) and imaged with a Leica DM5500B microscope (Leica Microsystems, Buffalo Groove, IL) with a 63× oil immersion objective (Leica Microsystems). The sizes and circularities of cells and cell nuclei ($n > 20$ for each case) were quantified in ImageJ (NIH, Bethesda, MD) based on the F-actin and nucleus staining, respectively.

Cell stiffness measurements using AFM nanoindentation
The colloid probe was prepared by attaching a 5-μm sphere to the end of a triangular silicon nitride cantilever as detailed previously.[36] A multimode AFM with a Nanoscope IIIa control system and scanner-J (software version 5.31r1, Veeco Instruments, Santa Barbara, CA) was used to measure the mechanics of cells. Indentation was performed with force–volume image mode over an area of 30 μm × 30 μm under buffer solution in a fluid cell. The images produced by this mode consist of an array of position–deflection curves and a corresponding topographic map. All force maps were acquired at a scan rate of 1 Hz and piezo ramp size of 1500 nm with an array of 32 × 32 force curves. The trigger mode was set at a relative deflection threshold of

100 nm. The Young's modulus (E) was computed from approaching force curves using a Hertzian model described previously.[38]

Fluorescence lifetime measurement

Cell membranes were stained with 1,1'-didodecyl-3,3,3',3'-tetramethylindocarbocyanine perchlorate (DiI-C_{12}; Invitrogen, Eugene, OR) at a concentration of 1.0 μM for 4–5 min at 37 °C. After staining, cells were extensively washed with Dulbecco's phosphate-buffered saline (DPBS) and left in phenol-red free Dulbecco's modified eagle medium (DMEM) with 10% FBS. The fluorescence lifetime of DiI-C_{12} was measured using the TCSPC technique. The system setup and theoretical basis were described in detail elsewhere.[39] The laser position with respect to the imaging system was marked by checking the photobleaching spot on a DiI-covered coverslip before each experiment. The instrument response function (IRF) was collected using a sample of 0.2 M Rhodamine 6G solution (Invitrogen, Eugene, OR), prior to the experiment.[40] The laser was positioned on each cell based on the fluorescence images under a 60× water-immersed objective (NA = 1.20, UPlanApo; Olympus, Tokyo, Japan). Special attention was paid to make sure the photons collected were actually from the apical membrane by noting the peak in fluorescence on the top cell surface during a z-scan. The decay curves were fitted to a decay model with two exponentials. The curve fitting was performed using Fluofit software (PicoQuantGmbh, Berlin, Germany). The average value of five independent replicas of two independent experiments for each case was reported with the standard deviation.

Flow cytometry

Cells were seeded at a density of 1000 cell/cm^2 on both smooth and fibrous substrates. The medium was replaced with fresh medium containing orange carboxylate-modified fluorescent polystyrene NPs (100 nm; Invitrogen, Eugene, OR) at 0.02 mg/mL after an initial 24 h to permit cell attachment and cell–substrate interaction. Detailed information on the NPs is available at the company web site. Prior to loading, the NPs were sonicated for 15 min to break apart aggregates. Cells were incubated with NPs for 6 h to allow the cellular uptake to reach equilibrium, and then rinsed three times with PBS to remove extracellular NPs. Cells were then harvested with 0.05% trypsin–EDTA, followed by neutralizing using fresh growth medium and centrifuging at 300g for 4 min. After discarding the supernatant, the cell pellet was fixed and homogenized using 3.7% paraformaldehyde in PBS and pipetted up/down several times until a homogenous single cell suspension was obtained for flow cytometry experiments. Intracellular fluorescence intensity was measured using a GUAVA flow cytometer with a PT-1 orange emission filter ($\geq$10,000 events were collected in each measurement). The average value of three independent replicas of two independent experiments for each case was reported with the standard deviation.

Inhibition of cytoskeletal organization and contractility

We designed our inhibition experiments by following the manufacturer's protocols as well as previously published
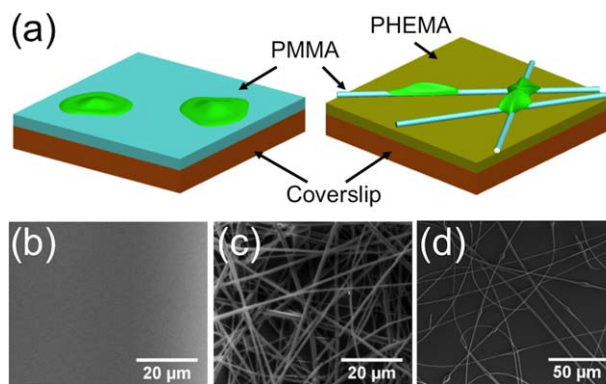
FIGURE 1. (a) Schematics of cells seeded on completely flat and fibrous substrates. For the fibrous substrates, cells are only adherent to PMMA fibers, but not to the precoated PHEMA layer. Representative SEM images of the substrates with various surface topographic features: flat (b), with dense fibers (c), and with sparse fibers (d). [Color figure can be viewed in the online issue, which is available at wileyonlinelibrary.com.]

studies for various cell lines to understand endocytic transport mechanisms.[41–44] Prior to each flow cytometry experiment the cellular viability and overall phenotype were confirmed under an optical microscope. Briefly, cells were seeded on both flat and fibrous substrates and cultured for 24 h as described above. Prior to loading NPs, cells were treated with either blebbistatin (Sigma-Aldrich) which inhibits the ATPase function of nonmuscle MyosinII or cytochalasin D which caps the barbed end of F-actin polymers and therefore inhibits the F-actin polymerization (Sigma-Aldrich) for 30 min at a concentration of 10 μM and 10 μg/mL, respectively. After the treatment, cells were incubated with NPs for 6 h, followed by flow cytometry to quantify cellular uptake as described above.

Statistical analysis

Data are represented as mean $\pm$ standard deviation. Student's *t-test* was performed where statistical significance of the difference in means between two groups was tested. A 95% confidence level (p values <0.05) was considered to be statistically significant. Due to the non-normal distribution of the AFM data, Kruskal–Wallis one-way analysis of variance test by ranks was performed on mean Young's modulus values for statistical significance.[45]

RESULTS

For our experiments, completely flat and fibrous surfaces were prepared for cell seeding (Figure 1). The flat substrate was prepared by spin-coating 2% PMMA onto 22 mm × 22 mm glass slides [Figure 1(b)]. To fabricate fibrous substrates, PMMA fibers were deposited onto glass slides of the same dimensions via electrospinning. The glass slides were precoated with PHEMA in order to inhibit cell adhesion on nonfibrous regions [Figure 1(a)]. The fiber density can be well controlled by varying the deposition time during electrospinning. The fiber densities in our studies were chosen such that multiple fibers were underneath each cell for the dense case (60 s deposition), while only a single fiber for
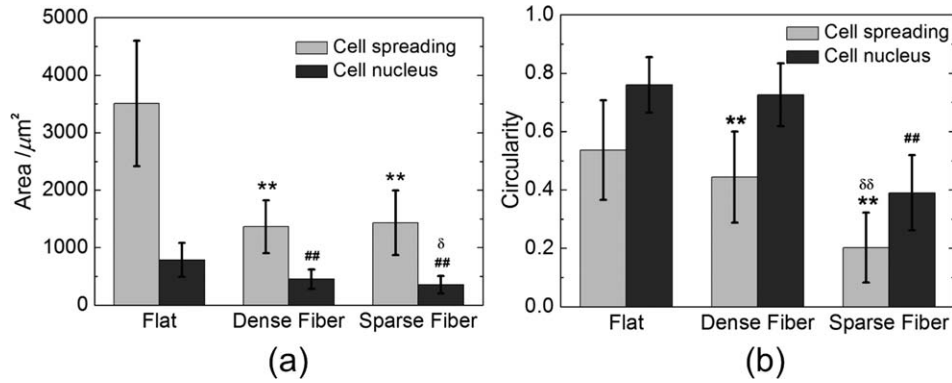
FIGURE 2. Cell responses to substrate topography. (a) Cell spreading area and cell nucleus size vary with substrate surface topographies. (b) Circularities of cell spreading and nuclei vary with substrate surface topographies. **Significance at $p < 0.01$ with respect to the cell spreading on flat substrates. ##Significance at $p < 0.01$ with respect to the cell nucleus on flat substrates. δSignificance at $p < 0.05$ with respect to the cell nucleus on dense fiber substrates. δδSignificance at $p < 0.01$ with respect to the cell spreading on dense fiber substrates.

the sparse case [10 s deposition; Figure 1(c,d)]. Our experimental settings allowed us to fabricate uniform PMMA fibers with an average diameter of 1.64 ± 0.31 μm, as measured using SEM. Using AFM, the stiffnesses of the flat PMMA layer and PMMA fibers were measured, and found to fall within the range of ~1.8–3.0 GPa. The comparable stiffness of the flat PMMA layer and fibers decouples the effect of surface topography from substrate stiffness. The topographies of both flat and fibrous substrates were further examined using SEM prior to cell seeding.

Prior to imaging and other treatments, cells were seeded on both flat and fibrous substrates and cultured for 24 h to allow focal adhesions to be fully developed and stabilized. Compared with cells on the flat PMMA surface, the spreading level and the size of cell nucleus on the fibrous substrates were reduced by 2.5 and 2.0 times [Figure 2(a)], respectively. Though the degrees of cell spreading on the dense and sparse fiber substrates remained roughly the same, the cell nuclei on the sparse fiber substrates were relatively smaller. On the flat substrates, cells did not show any preference in the direction of polarization, since all directions were topographically invariant. In contrast, cells could only spread along the fibers on fibrous substrates and therefore cell morphologies were determined by the fiber patterns. We used circularity as an indicator of the polarization level of the cells, defined by $C = 4A\pi/L^2$, where A and L are the spreading area and perimeter of the cells, respectively. Note that $C = 1$ corresponds to the perfectly circular shape. As the value of C approaches zero, the cell becomes highly polarized and its shape significantly deviates from a perfect circle (such as the needle-like shape). Our measurements indicated that cells on fibrous substrates were significantly less circular than those on flat substrates, especially on sparse fibers [Figure 2(b)]. Though cell outlines on flat substrates were more circular than those on dense fibers, the circularities of cell nuclei on flat and dense fiber substrates showed negligible difference. However, the cell nuclei on sparse fiber substrates were significantly less circular than those on flat and dense fiber substrates.

Fluorescence immunostaining was performed to visualize cell spreading and morphology in response to various surface topographies by simultaneously staining F-actin, vinculin, and cell nuclei (Figure 3). Cell nuclei exhibited distinct patterns on different substrates. On the flat surface, cell nuclei were mostly elliptical with smooth boundaries, while they were more irregularly shaped due to the spatial confinement from multiple fibers on dense fiber substrates. They unidirectionally elongated along the fibers on sparse fiber substrates, forming a spindle shape. Phalloidin staining of F-actin clearly demonstrated well-aligned stress fibers within cells on the flat surface, while much thicker stress fiber bundles formed along the edges of spindle-shaped cells on sparse fiber substrates. Compared with the cells on the flat and sparse fiber substrates, fewer aligned stress fibers were formed on dense fiber substrates. Vinculin staining showed that large focal adhesion sites were formed wherever cells adhered to fibers (see white arrows in Figure 3), indicating that fibers promote focal adhesion formation and maturation.

The distinct phenotypes of the cells inspired further examination of cell mechanics on various substrates, including the membrane tension and elastic modulus of the cells, thereby establishing the mechanics–morphology relationship. It has been reported that membrane tension is a critically important factor for the cellular uptake of NPs via endocytosis.[15] Using the time-correlated single-photon counting (TCSPC) technique we measured the membrane tension of cells on various substrates. This method has been described in details and validated elsewhere.[39,46,47] Briefly, a lipophilic dye (e.g., DiI) is used to stain cell membrane, which is embedded into the hydrophobic tails of phospholipids due to the hydrophobic interactions. The lifetime of the fluorescent dye after being excited by a laser is an indicator of the membrane tension level because its nonradiative decay is correlated to the extent of the dye molecule exposure to water, that is, the free area occupied by the dye molecule. The larger the free area, the higher the membrane tension, and the shorter the fluorescence lifetime of the dye. Figure 4 shows that the membrane tension of the cells

	Phase Contrast	DAPI	Phalloidin	Vinculin	Merged
Flat					
Dense fiber					
Sparse fiber					
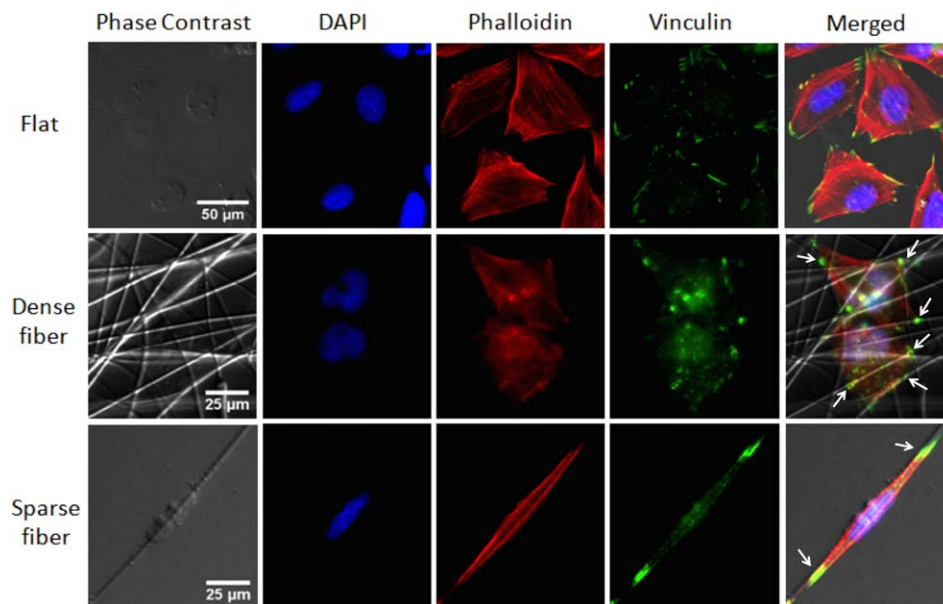
FIGURE 3. Representative fluorescence images of SaOS-2 cells on various substrates with distinct surface topographies. [Color figure can be viewed in the online issue, which is available at wileyonlinelibrary.com.]

grown on dense fiber substrates was lower than that on flat and sparse fiber substrates, while the cells on flat substrates were at the highest tension level.

We further measured cell moduli on different substrates using AFM. Our measurements revealed a clear difference in the overall elastic moduli between cells grown on sparse fiber substrates and those on the dense fiber and flat substrates (Figure 5). The mean elastic modulus of the cells on sparse fibers was more than ~25% higher than flat counterparts and more than ~30% higher than the cells grown on dense fibers. Whereas the measured mean moduli for cells grown on dense fiber substrates and flat substrates differ only by ~6%. According to Kruskal–Wallis significance test,[45] the differences between any two groups were statistically significant. Our analyses further show that the median moduli followed the same trend as the mean moduli, as pre-

viously described. It is worth noting the direct correlation between stress fiber formation within cells and the overall elastic modulus of the cells: the thicker the stress fiber bundles, the higher stiffness of the cells. This observation is consistent with our previous report that dense stress fibers were correlated with elastic modulus increase on fibrous topographies in osteoblasts.[48] It should also be noted that both membrane tension and stress fiber contribute to the cell moduli. The higher moduli but lower membrane tension of the cells grown on sparse fibers than those of cells on flat substrates indicate the dominant role of the stress fiber formation on the cell moduli.

We next used 100 nm carboxylate-modified fluorescent polystyrene NPs (COOH-NPs) to investigate the roles of the substrate topography on the cellular uptake of NPs. The bright and stable fluorescent signal of the NPs facilitated
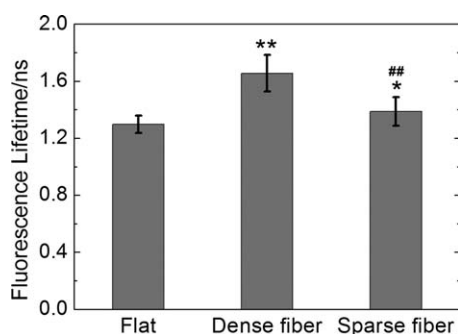
FIGURE 4. Fluorescence lifetime of DiI-C_{12} on substrates of various surface topographies. The mean lifetime on flat PMMA, dense fiber and sparse fiber substrates are 1.30 ± 0.06 ns, 1.66 ± 0.13 ns, and 1.38 ± 0.10 ns, respectively. **Significance at $p < 0.01$ and *significance at $p < 0.05$ with respect to the fluorescence lifetime on flat substrates. ##Significance at $p < 0.01$ with respect to the fluorescence lifetime on dense fiber substrates.
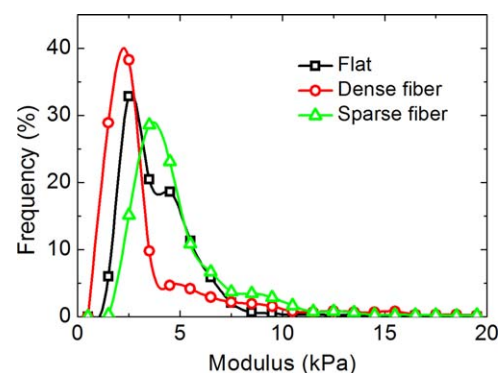
FIGURE 5. Distribution of elastic moduli of cellular apical surface on substrates of various surface topographies measured using AFM. The mean moduli on flat PMMA, dense fiber and sparse fiber substrates are 3.94 ± 1.90 kPa, 3.62 ± 3.12 kPa, and 4.99 ± 2.60 kPa, respectively. [Color figure can be viewed in the online issue, which is available at wileyonlinelibrary.com.]
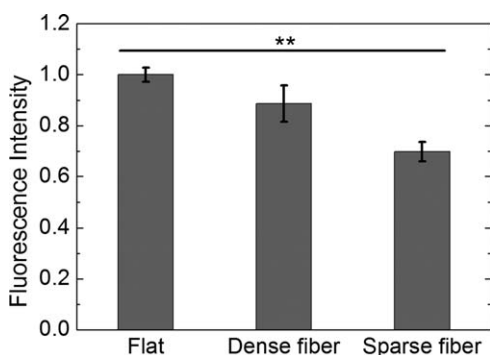
FIGURE 6. Cellular uptake of fluorescent NPs by cells on substrates of different surface topographies. The fluorescence intensities are normalized by the intensity on flat PMMA surface. **Significance at $p < 0.01$ between any two groups.

the quantification of the cellular uptake level via flow cytometry (see Materials and Methods). To ensure that only NPs inside cells contributed to flow cytometry signals, cells were extensively washed to completely remove free NPs in the solution and those adhered on cell surface after 6-h incubation.[15] Figure 6 shows that the cellular uptake of NPs on sparse fiber substrates was reduced by about 30% as compared with the cells on the flat PMMA substrates. Our previous theoretical analyses have revealed that both membrane tension and spreading area affect cellular uptake of NPs.[15] Our TCSPC measurements have clearly shown that membrane tension is higher on the flat surface. Therefore, it follows that the reduction in cellular uptake of NPs on fibrous substrates was caused by the reduced spreading level of the cells. Though cells displayed insignificant difference in the spreading area between dense and sparse fiber substrates [Figure 2(a)], the higher membrane tension resulted in lower uptake level in the cells on sparse fiber substrates. Normalizing the cellular uptake by the spreading area illustrated that the highest and lowest uptake efficiencies (per unit area) occur on dense fiber and flat substrates, respectively, which is consistent with the corresponding tension levels measured by TCSPC.

In order to investigate whether and how the substrate topography mediates the endocytic pathways, we measured and compared the cellular uptake of NPs on flat and fibrous substrates in the presence/absence of pharmacological inhibitors. Despite the possible cytotoxicity and complexity, pharmacological inhibitors provide a straightforward way to investigate endocytic pathways of NPs and have been widely used in in vitro studies.[43,49,50] Herein, sparse fiber substrates were adopted for our inhibition assays. We used blebbistatin, a myosin II inhibitor, and cytochalasin D, an actin polymerization inhibitor, to probe the possible roles of cell contractility and stress fiber formation in cellular uptake of NPs on different substrate topographies.

From a mechanics point of view, disrupting either cell contractility or actin polymerization decreases the cell stiffness and therefore would lower the resistance for cells to internalize NPs. However, our experiments showed that treating cells with either blebbistatin or cytochalasin D

inhibited cellular uptake of NPs on both flat and fibrous substrates (Figure 7). Though this result seemed to be counter-intuitive, it agrees with existing studies[51] and might be due to two possible reasons. First, treating cells with pharmaceutical drugs not only inhibits the formation of target structures but also may disrupt essential signaling and force transducing pathways that affect the overall morphology and mechanical properties of the cells; both in turn influence the cellular uptake. For example, we observed dramatic morphological change in cells in the presence of pharmaceutical inhibitors (results not shown). Second, studies have proposed the positive effects of stress fibers on endocytosis.[52] Stress fibers provide assistance for cell membrane to deform by pulling membrane inward during endocytosis and help vesicle scission to occur at the last stage of endocytosis. The cellular uptake reduction levels of the cells in the presence of blebbistatin and cytochalasin D differed on fibrous and flat substrates. The cellular uptake of cells on fibrous substrates was reduced by >30% with blebbistatin, but <15% with cytochalasin D, while both blebbistatin and cytochalasin D reduced the cellular uptake by 20% for cells on the flat substrates. This result indicates that substrate topography markedly regulates the roles of myosin II and stress fibers in the cellular uptake of NPs, wherein myosin II contractility is critical to NP uptake on fibrous substrates.

DISCUSSION

As ECMs in vivo vary widely in chemical compositions[33] (collagen, fibronectin, glycosaminoglaycans), organization (topography,[53,54] porosity[55]), and physical properties (stiffness[56]), it is critically important to design nanoscale targets in concert with the physicochemical properties of the ECM to achieve optimized targeting efficiency. To date, for therapeutic purposes, the roles of substrate physicochemical properties such as stiffness of the substrate[57] and surface chemistry[58] have been investigated in regards to the cellular response. Likewise, the optimization of the physicochemical properties of the NPs for targeted delivery has been heavily studied.[59] However, the effects of the local physical environments of the
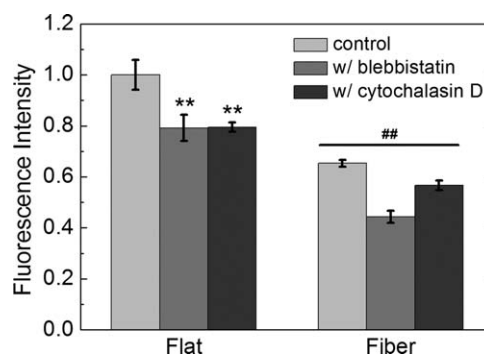
FIGURE 7. Effects of pharmacological inhibitors on the cellular uptake of NPs on both flat and fibrous substrates. The fluorescence intensities are normalized by the intensity on flat PMMA surface without any inhibitor. **Significance at $p < 0.01$ with respect to the control case on flat substrates. ##Significance at $p < 0.01$ between any two groups.

cells, such as topography, on the cellular uptake of NPs are largely omitted from current literature.

Our study provided clear evidence for the first time that substrate topography modifies the mechanical properties and morphologies of the cells, which in turn modulates the uptake efficiency of NPs. In particular, our results showed that seeding cells on fibrous substrates with different fiber densities alters cellular morphology and cytoskeletal organization, leading to the changes in the overall stiffness of the cells as well as membrane tension level. We found that the NP uptake efficiency changes consistently with the phenotypic and mechanical properties of the cells. Our inhibition studies showed that disrupting the acto-myosin coupling through blebbistatin and cytochalasin D inhibits the uptake efficiency, consistent with previous studies.[51] Our results further indicated that the impact of intracellular structures on the cellular uptake efficiency vary on different surface topographies. Namely, myosin II is more critical to the cellular uptake of NP on fibrous substrates than actin fibers, while the effects of myosin II and actin are on the same level on flat substrates. The mechanistic understanding on the surface topography-mediated cellular uptake of NPs opens a new dimension for the rational design of NP-based drug delivery nanocarriers for improved cellular targeting.

REFERENCES

1. Aoyama Y, Kanamori T, Nakai T, Sasaki T, Horiuchi S, Sando S, Niidome T. Artificial viruses and their application to gene delivery. size-controlled gene coating with glycocluster nanoparticles. J Am Chem Soc 2003;125:3455–3457.
2. Chithrani BD, Ghazani AA, Chan WCW. Determining the size and shape dependence of gold nanoparticle uptake into mammalian cells. Nano Lett 2006;6:662–668.
3. Gao HJ, Shi WD, Freund LB. Mechanics of receptor-mediated endocytosis. Proc Natl Acad Sci USA 2005;102:9469–9474.
4. Jiang W, Kim BYS, Rutka JT, Chan WCW. Nanoparticle-mediated cellular response is size-dependent. Nat Nanotechnol 2008;3:145–150.
5. Osaki F, Kanamori T, Sando S, Sera T, Aoyama Y. A quantum dot conjugated sugar ball and its cellular uptake on the size effects of endocytosis in the subviral region. J Am Chem Soc 2004;126:6520–6521.
6. Zhang S, Li J, Lykotrafitis G, Bao G, Suresh S. Size-dependent endocytosis of nanoparticles. Adv Mater 2009;21:419–424.
7. Gratton SEA, Ropp PA, Pohlhaus PD, Luft JC, Madden VJ, Napier ME, DeSimone JM. The effect of particle design on cellular internalization pathways. Proc Natl Acad Sci USA 2008;105:11613–11618.
8. Huang C, Zhang Y, Yuan H, Gao H, Zhang S. Role of nanoparticle geometry in endocytosis: Laying down to stand up. Nano Lett 2013;13:4546–4550.
9. Huang X, Teng X, Chen D, Tang F, He J. The effect of the shape of mesoporous silica nanoparticles on cellular uptake and cell function. Biomaterials 2010;31:438–448.
10. Bergen JM, Von Recum HA, Goodman TT, Massey AP, Pun SH. Gold nanoparticles as a versatile platform for optimizing physicochemical parameters for targeted drug delivery. Macromol Biosci 2006;6:506–516.
11. Tong S, Hou S, Ren B, Zheng Z, Bao G. Self-assembly of phospholipid–PEG coating on nanoparticles through dual solvent exchange. Nano Lett 2011;11:3720–3726.
12. Yuan HY, Huang CJ, Zhang SL. Virus-inspired design principles of nanoparticle-based bioagents. PLoS One 2010;5:e13495.
13. Yuan HY, Li J, Bao G, Zhang SL. Variable nanoparticle–cell adhesion strength regulates cellular uptake. Phys Rev Lett 2010;105:138101–138104.
14. Han J, Zern BJ, Shuvaev VV, Davies PF, Muro S, Muzykantov V. Acute and chronic shear stress differently regulate endothelial internalization of nanocarriers targeted to platelet–endothelial cell adhesion molecule-1. Acs Nano 2012;6:8824–8836.
15. Huang C, Butler PJ, Tong S, Muddana HS, Bao G, Zhang S. Substrate stiffness regulates cellular uptake of nanoparticles. Nano Lett 2013;13:1611–1615.
16. Kong HJ, Liu JD, Riddle K, Matsumoto T, Leach K, Mooney DJ. Non-viral gene delivery regulated by stiffness of cell adhesion substrates. Nat Mater 2005;4:460–464.
17. Lin A, Sabnis A, Kona S, Nattama S, Patel H, Dong J-F, Nguyen KT. Shear-regulated uptake of nanoparticles by endothelial cells and development of endothelial-targeting nanoparticles. J Biomed Mater Res Part A 2010;93A:833–842.
18. Samuel SP, Jain N, O'Dowd F, Paul T, Kashanin D, Gerard VA, Gun'ko YK, Prina-Mello A, Volkov Y. Multifactorial determinants that govern nanoparticle uptake by human endothelial cells under flow. Int J Nanomed 2012;7:2943–2956.
19. Biggs MJP, Richards RG, Gadegaard N, McMurray RJ, Affrossman S, Wilkinson CDW, Oreffo ROC, Dalby MJ. Interactions with nanoscale topography: Adhesion quantification and signal transduction in cells of osteogenic and multipotent lineage. J Biomed Mater Res Part A 2009;91A:195–208.
20. Chan CK, Liao S, Li B, Lareu RR, Larrick JW, Ramakrishna S, Raghunath M. Early adhesive behavior of bone-marrow-derived mesenchymal stem cells on collagen electrospun fibers. Biomed Mater 2009:4.
21. Lim JY, Dreiss AD, Zhou ZY, Hansen JC, Siedlecki CA, Hengstebeck RW, Cheng J, Winograd N, Donahue HJ. The regulation of integrin-mediated osteoblast focal adhesion and focal adhesion kinase expression by nanoscale topography. Biomaterials 2007;28:1787–1797.
22. Brunette DM, Chehroudi B. The effects of the surface topography of micromachined titanium substrata on cell behavior in vitro and in vivo. J Biomech Eng-T ASME 1999;121:49–57.
23. Clark P, Connolly P, Curtis ASG, Dow JAT, Wilkinson CDW. Cell guidance by ultrafine topography in vitro. J Cell Sci 1991;99:73–77.
24. Li S, Guan JL, Chien S. Biochemistry and biomechanics of cell motility. Annu Rev Biomed Eng 2005:105–150.
25. Miller DC, Thapa A, Haberstroh KM, Webster TJ. Endothelial and vascular smooth muscle cell function on poly(lactic-co-glycolic acid) with nano-structured surface features. Biomaterials 2004;25:53–61.
26. Washburn NR, Yamada KM, Simon CG, Kennedy SB, Amis EJ. High-throughput investigation of osteoblast response to polymer crystallinity: Influence of nanometer-scale roughness on proliferation. Biomaterials 2004;25:1215–1224.
27. Zhu XL, Chen J, Scheideler L, Reichl R, Geis-Gerstorfer J. Effects of topography and composition of titanium surface oxides on osteoblast responses. Biomaterials 2004;25:4087–4103.
28. Christopherson GT, Song H, Mao HQ. The influence of fiber diameter of electrospun substrates on neural stem cell differentiation and proliferation. Biomaterials 2009;30:556–564.
29. Vogel V, Sheetz M. Local force and geometry sensing regulate cell functions. Nat Rev Mol Cell Biol 2006;7:265–275.
30. Yim EKF, Pang SW, Leong KW. Synthetic nanostructures inducing differentiation of human mesenchymal stem cells into neuronal lineage. Exp Cell Res 2007;313:1820–1829.
31. Curtis ASG. Control of cell behavior—topological factors. J Natl Cancer Inst 1964;33:15-&.
32. Nikkhah M, Edalat F, Manoucheri S, Khademhosseini A. Engineering microscale topographies to control the cell–substrate interface. Biomaterials 2012;33:5230–5246.
33. Alberts B, Johnson A, Lewis J, Ralf M, Roberts K, Walter P. Molecular Biology of the Cell. New York: Garland; 2002.
34. Lim SH, Liu XY, Song HJ, Yarema KJ, Mao HQ. The effect of nanofiber-guided cell alignment on the preferential differentiation of neural stem cells. Biomaterials 2010;31:9031–9039.
35. Wang HB, Mullins ME, Cregg JM, McCarthy CW, Gilbert RJ. Varying the diameter of aligned electrospun fibers alters neurite outgrowth and Schwann cell migration. Acta Biomater 2010;6:2970–2978.

36. Li X, Logan BE. Analysis of bacterial adhesion using a gradient force analysis method and colloid probe atomic force microscopy. Langmuir 2004;20:8817–8822.
37. Jaiswal D, Brown JL. Nanofiber diameter-dependent MAPK activity in osteoblasts. J Biomed Mater Res A 2012;100:2921–2928.
38. Hansen JC, Lim JY, Xu LC, Siedlecki CA, Mauger DT, Donahue HJ. Effect of surface nanoscale topography on elastic modulus of individual osteoblastic cells as determined by atomic force microscopy. J Biomech 2007;40:2865–2871.
39. Gullapalli RR, Tabouillot T, Mathura R, Dangaria JH, Butler PJ. Integrated multimodal microscopy, time-resolved fluorescence, and optical-trap rheometry: Toward single molecule mechanobiology. J Biomed Opt 2007;12:014012.
40. Penzkofer A, Lu Y. Fluorescence quenching of rhodamine 6g in methanol at high-concentration. Chem Phys 1986;103:399–405.
41. Arnsdorf EJ, Tummala P, Kwon RY, Jacobs CR. Mechanically induced osteogenic differentiation—The role of RhoA, ROCKII and cytoskeletal dynamics. J Cell Sci 2009;122:546–553.
42. Kitchens KM, Kolhatkar RB, Swaan PW, Ghandehari H. Endocytosis inhibitors prevent poly(amidoamine) dendrimer internalization and permeability across Caco-2 cells. Mol Pharm 2008;5:364–369.
43. Sato K, Nagai J, Mitsui N, Ryoko Y, Takano M. Effects of endocytosis inhibitors on internalization of human IgG by Caco-2 human intestinal epithelial cells. Life Sci ;85:800–807.
44. Vercauteren D, Vandenbroucke RE, Jones AT, Rejman J, Demeester J, De Smedt SC, Sanders NN, Braeckmans K. The use of inhibitors to study endocytic pathways of gene carriers: Optimization and pitfalls. Mol Ther 2010;18:561–569.
45. Bongiorno T, Kazlow J, Mezencev R, Griffiths S, Olivares-Navarrete R, McDonald JF, Schwartz Z, Boyan BD, McDevitt TC, Sulchek T. Mechanical stiffness as an improved single-cell indicator of osteoblastic human mesenchymal stem cell differentiation. J Biomech 2013;47:2197–2204.
46. Muddana HS, Gullapalli RR, Manias E, Butler PJ. Atomistic simulation of lipid and Dil dynamics in membrane bilayers under tension. Phys Chem Chem Phys 2011;13:1368–1378.
47. Tabouillot T, Muddana HS, Butler PJ. Endothelial cell membrane sensitivity to shear stress is lipid domain dependent. Cell Mol Bioeng 2011;4:169–181.
48. Ozdemir T, Xu LC, Siedlecki C, Brown JL. Substrate curvature sensing through myosin IIa upregulates early osteogenesis. Integr Biol (Camb) 2013;5:1407–1416.
49. Zhang LW, Baumer W, Monteiro-Riviere NA. Cellular uptake mechanisms and toxicity of quantum dots in dendritic cells. Nanomedicine (Lond) 2011;6:777–791.
50. Zhang LW, Monteiro-Riviere NA. Mechanisms of quantum dot nanoparticle cellular uptake. Toxicol Sci 2009;110:138–155.
51. dos Santos T, Varela J, Lynch I, Salvati A, Dawson KA. Effects of transport inhibitors on the cellular uptake of carboxylated polystyrene nanoparticles in different cell lines. PLoS One 2011;6:10.
52. Kaksonen M, Toret CP, Drubin DG. Harnessing actin dynamics for clathrin-mediated endocytosis. Nat Rev Mol Cell Biol ;7:404–414.
53. McBeath R, Pirone DM, Nelson CM, Bhadriraju K, Chen CS. Cell shape, cytoskeletal tension, and RhoA regulate stem cell lineage commitment. Dev Cell 2004;6:483–495.
54. Ozdemir T, Higgins AM, Brown JL. Osteoinductive biomaterial geometries for bone regenerative engineering. Curr Pharm Des 2013;19:3446–3455.
55. Brown JL, Peach MS, Nair LS, Kumbar SG, Laurencin CT. Composite scaffolds: Bridging nanofiber and microsphere architectures to improve bioactivity of mechanically competent constructs. J Biomed Mater Res A 2010;95:1150–1158.
56. Discher DE, Janmey P, Wang Y-l. Tissue cells feel and respond to the stiffness of their substrate. Science 2005;310:1139–1143.
57. Engler AJ, Sen S, Sweeney HL, Discher DE. Matrix elasticity directs stem cell lineage specification. Cell ;126:677–689.
58. Keselowsky BG, Collard DM, Garcia AJ. Surface chemistry modulates focal adhesion composition and signaling through changes in integrin binding. Biomaterials 2004;25:5947–5954.
59. Treuel L, Jiang X, Nienhaus GU. New views on cellular uptake and trafficking of manufactured nanoparticles. J R Soc Interface 2013;10:20120939.